Journal of the European Ceramic Society 19 (1999) 2849–2858

PII: S0955-2219(99)00063-1
0955-2219/99/$ - see front matter

Thermal Evolution and Crystallisation of Polydimethylsiloxane–Zirconia Nanocomposites Prepared by the Sol–Gel Method

Sandra Dirè,[a]* Riccardo Ceccato,[a] Stefano Gialanella[a] and Florence Babonneau[b]

[a]Dipartimento di Ingegneria dei Materiali, Università di Trento, Via Mesiano 77, 38050 Trento, Italy
[b]Chimie de la Matière Condensée, Université Pierre et Marie Curie, 4 place Jussieu, 75252 Paris, France

(Received 1 July 1998; accepted 27 February 1999)

Abstract

Polydimethylsiloxane–zirconia nanocomposites have been prepared by hydrolysis of diethoxydimethylsilane and zirconium n-*propoxide in different molar ratios. Transparent, homogeneous and non-porous xerogels have been obtained up to 70 mol% ZrO_2 content. The starting xerogels have been pyrolyzed under argon atmosphere up to 1400°C and the structural evolution of samples treated at different temperatures has been followed by X-ray diffraction, transmission electron microscopy, infrared and ^{29}Si solid state nuclear magnetic resonance spectroscopies, thermal analyses and N_2 sorption measurements. The polymer-to-ceramic conversion leads to the structural rearrangement of the siloxane component with the production at 600°C of high surface area materials with pore sizes below 3 nm. Samples are amorphous up to 800°C. At 1000°C, the structural evolution of the silicon moiety produces an amorphous oxycarbide phase whereas the primary crystallisation of tetragonal zirconia takes place, with crystallinity and crystallite sizes depending on the ZrO_2 content. At 1400°C, the silicon oxycarbide phase generates a mixture of amorphous silica and crystalline silicon carbide polymorphs. In this matrix, tetragonal and monoclinic ZrO_2 phases are present with ZrO_2 average crystallite dimensions never exceeding 20 nm, for ZrO_2 content $\leq$50 mol%. The tetragonal/monoclinic ratio as well as the crystallite sizes appear strictly related to the chemical composition.* © *1999 Elsevier Science Ltd. All rights reserved*

Keywords: precursors-organic, sol–gel processes, nanocomposites, SiC, ZrO_2.

*To whom correspondence should be addressed.

1 Introduction

The sol–gel process is a well-known chemical route to prepare oxide-based materials which can be converted into glasses and ceramics by thermal treatments.[1] Moreover, the use of molecular precursors and the control of the synthesis conditions make it possible to prepare homogeneous and pure multicomponent systems.[2–4]

Over the last years, the sol–gel process has been extensively employed for the preparation of hybrid organic–inorganic materials, known as ormocers[5,6] or ceramers,[7,8] by modifying the oxide network with the introduction of organic functions. Organic–inorganic hybrid networks can be generated using several synthetic approaches by incorporating different inorganic and organic groups with variable structure.[8] A popular synthesis technique is based on the use of monomeric organoalkoxysilanes as precursors for the sol–gel reactions.[5,9,10] In this case, the organic groups are introduced within the inorganic network through the use of compounds like $R'_nSi(OR)_{4-n}$ ($n=1,2$), owing to the stability of the Si–C bond with respect to hydrolysis.

Recently, this approach has been successfully applied to the preparation of hybrid materials whose inorganic counterpart is generated by transition metal alkoxides (TMA), the organic modifier being diethoxydimethylsilane (DEDMS).[11–15] The interaction of DEDMS with TMA, during the first stages of the hydrolysis process, leads to the formation of intermediates containing heterometallic Si–O–M bonds (M = Ti, Zr),[16,17] finally yielding to polysiloxanes. DEDMS–TMA derived xerogels have been definitely described as composed of polydimethylsiloxane chains cross-linked by oxide particles, which should be nanometric in size according to the transparency of samples and X-ray absorption and SAXS results.[11,14,17]

The siloxane–oxide systems are attractive for a large variety of applications such as scratch resistant or hydrophobic coatings[18,19] and microporous materials.[20] Moreover, the siloxane-oxide xerogels are expected to be good preceramic materials that can be converted into oxycarbide glasses[21–25] or carbide composites[26,27] by pyrolysis under reducing atmosphere, owing to the high carbon load retained in the gel network. Some preliminary results have been presented on the pyrolytic conversion of $(CH_3)_2SiO$–TiO_2 xerogels leading to the production at high temperature of silica and titanium carbide based composites.[28]

The aim of this paper is to study the thermal evolution and crystallisation of polydimethylsiloxane–zirconia nanocomposites prepared using diethoxydimethylsilane and zirconium *n*-propoxide in different molar ratios. The structural evolution of the xerogels will be followed during the pyrolysis up to 1400°C under Ar atmosphere and the final ceramics will be characterised by spectroscopic techniques, surface area measurements, X-ray diffraction and electron microscopy.

2 Experimental

A solution of DEDMS (D), absolute ethanol and acidified water (pH = 1; HCl) in 1:1:1 molar ratio was allowed to react for three minutes before adding the appropriate amounts of $Zr(OPr^n)_4$ (ZR), in order to prepare DZR*x* sols with $x = Zr/(Zr + Si)$ molar ratio ranging from 10 to 70%. The homogeneous sols were cast in polypropylene vessels and gave transparent gels which were dried in air at 25°C for 2 weeks before the thermal treatments. The DZR*x* xerogels were heated under Ar at different temperatures up to 1400°C with a heating rate of 1°C min^{-1}.

After the thermal treatments, the samples were ground to powder in an agate mortar. Transmission electron microscopy (TEM) observations were conducted at 120 KeV with powder specimens spread on a copper grid covered with an amorphous carbon film. FTIR spectra were recorded in transmission mode on KBr pellets using a Nicolet 5DXC spectrometer, collecting 64 scans in the 4000–400 cm^{-1} range, with 2 cm^{-1} resolution. ^{29}Si MAS NMR spectra were recorded on a Bruker MSL 400 spectrometer with pulse width and delay between pulses of 2 μs and 60 s, respectively. Peaks are labelled according to the conventional notation: M, D, T and Q refer to $SiC_{4-x}O_x$ units with $x = 1$, 2, 3 and 4 respectively. N_2 sorption experiments were carried out at 77 K on a Sorptomatic 1800-Carlo Erba instrument. Powdered samples (350 mg) were degassed overnight at 80°C before analysis. The Kelvin equation was used for calculating the pore size distribution; surface area evaluation was obtained by the BET equation which was linear in the interval $0{\cdot}05 \leq p/p0 \leq 0{\cdot}33$ with a least-squares fit of 0·998. Thermogravimetric and differential thermal analyses (TGA and DTA) were performed on a Netzsch STA 409 thermobalance under 100 cc/min^{-1} Ar flow and with 10°C min^{-1} heating rate. XRD spectra were collected on a Rigaku DMax diffractometer in the Bragg-Brentano configuration, using Cu K_α radiation and a monochromator on the diffracted beam. A modified Rietveld method program[29] was employed for the quantitative phase analysis and the evaluation of the average crystallite dimensions.

3 Results

3.1 FTIR spectroscopy

The evolution of the FTIR spectra is studied as a function of the pyrolysis temperature. The main peaks that will be discussed are summarized in Table 1. Figure 1 presents the results obtained for the DZR10 sample. As reported elsewhere,[30] the spectrum of the xerogel is characterised by the presence of the Si–O vibrations, typical of D units (1017 and 1096 cm^{-1}), and of the signals due to the methyl groups bonded to silicon (1263, 865 and 798 cm^{-1}). For DZR10, this structural situation appears unchanged up to 400°C whereas at 600°C remarkable network modifications[30] have already taken place, resulting in the intensity reduction of the Si–CH_3 absorptions and the strong changes in the Si–O stretching vibrations, now present as a single band centred at 1030 cm^{-1}. At 1000°C, the absorptions due to C–H and Si–CH_3 bonds disappear and the spectrum shows a broad band at 1038 cm^{-1}, indicative of a disordered silica based network, and a peak at 473 cm^{-1} due to the Si–O–Si absorption which presents a shoulder at 548 cm^{-1} attributed to the presence of a zirconia phase. At 1400°C, the DZR10 spectrum is characterised by intense and relatively sharp peaks due to the Si–O bonds at 1094 and 457 cm^{-1} together with the signal at 536 cm^{-1} due to an ordered ZrO_2 phase.[31] The intensity of the peak at 811 cm^{-1} is quite remarkable; it corresponds to the superposition of the broad signal due to silica and the sharp Si–C stretching in an ordered SiC phase, as confirmed by a comparison with a commercial polycrystalline SiC sample.

The evolution of the DZR20 and DZR30 spectra versus temperature is quite similar to the one presented for DZR10. On the contrary, significant structural differences are shown by DZR50 (Fig. 2), starting from the xerogel state. The overlapping of

Table 1. FTIR adsorption frequencies for selected peaks

*DZR*x, x	*Si–CH₃, cm⁻¹ (gel)*	*Si-O, cm⁻¹ (gel)*	*Si–O, cm⁻¹* (T, °C)	*Zr–O, cm⁻¹ (1400°C)*
10	1263	1096	1030 (600)	536
		1017	1038 (1000)	
			1095 (1400)	
50	1260	1044	1016 (600)	742
		1018[a]	1085 (1000)	588
		980[a]	1090 (1400)	494[c]
		933[a]		
70	1258	974[b]	1022 (600)	736
			1078 (1000)	581
			1074 (1400)	497[c]

[a]Contribution of Si–O–Zr and Si–OH bonds.
[b]Probable contribution of Si–O–Zr bonds.
[c]Overlapped with Si–O–Si absorption.

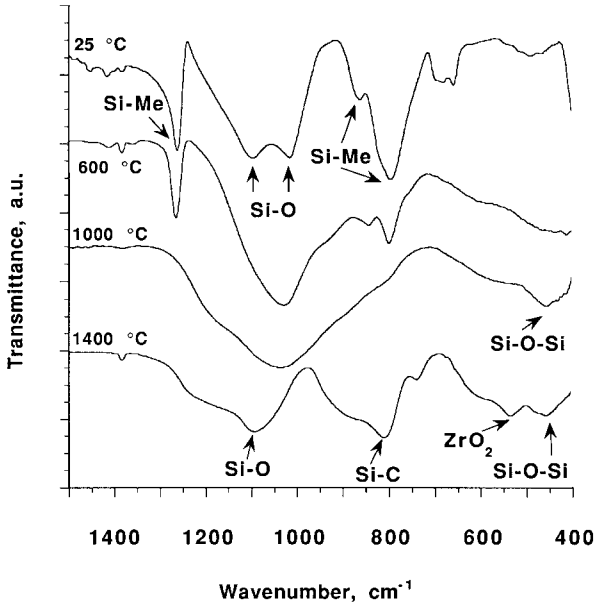

Fig. 1. Evolution with temperature of the FTIR spectra of the DZR10 samples.

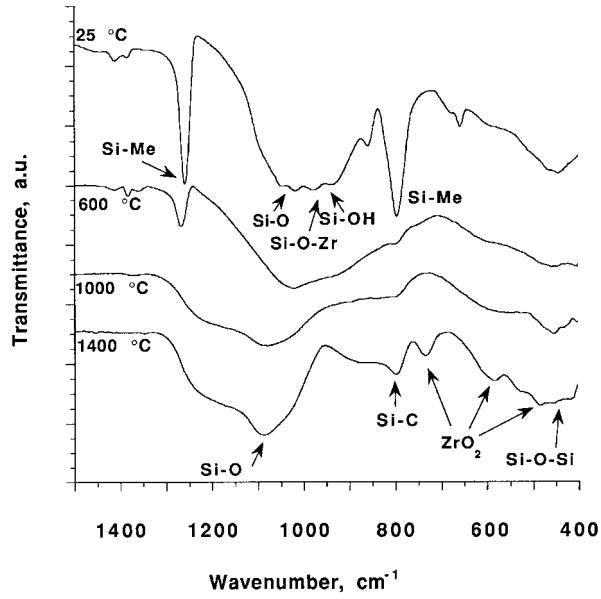

Fig. 2. Evolution with temperature of the FTIR spectra of the DZR50 samples.

at least four peaks (1044, 1018, 980 and 933 cm^{-1}) accounts for the Si–O and Si–OH absorptions together with the probable presence of Si–O–Zr bonds[32,33] in the xerogel. At 600°C, the pyrolysis process results in a more disordered network than the one shown by DZR10 at the same temperature whereas, at 1000°C, only slight differences can be found between the two samples. At 1400°C, the main peak at 1092 cm^{-1} is due to the silica phase. The Si–C absorption is less intense than in the case of DZR10 and shifted towards lower frequencies (796 cm^{-1}) and the absorptions related to zirconia at 742, 588 and 494 cm^{-1} are better defined.

Specific features are exhibited by the spectra of the DZR70 sample treated at different temperatures (Fig. 3). At room temperature, the signal due to the Si–CH_3 stretching is present at 1258 cm^{-1}, showing a low-frequency shift compared with reported results for DZRx with $x \leq 50$. The Si–O stretching vibrations appear at surprisingly low frequency (974 cm^{-1}) and the signals due to the Zr–O bonds are clearly visible at 608 and 453 cm^{-1}, with an overlap with the Si–O–Si vibration for the latter one. The pyrolysis process leads at higher temperature to the formation of a well defined ZrO_2 network[34] together with a disordered silica counterpart.

A comparison between the DZRx FTIR spectra recorded on samples pyrolysed at 1400°C points out the progressive inversion in intensity of the Si–O (1090 cm^{-1}) and Si–C (800 cm^{-1}) peaks (Fig. 4). As the ZrO_2 content increases, the relative amount of the SiC phase decreases and the Si–C stretching shifts towards a lower frequency, from 811 cm^{-1} for DZR10 to 796 cm^{-1} for DZR50. This could be an indication of differences in the nature of the SiC domains.

3.2 Thermal analyses and porosity

The weight losses, calculated from the TG curves carried out under Ar flow, are reported in Fig. 5 as a function of the ZrO_2 content. Two different steps are present in the TG curves and their intensity depends on the gel chemical composition. The first

weight loss (W_1) is found below 400°C and increases with the ZrO_2 content. The second weight loss (W_2), which takes place in the 400–900°C temperature range, decreases with increasing the ZrO_2 content. Similar behaviour is observed for the total weight loss (W_{tot}). Slightly different temperature ranges, corresponding to W_1 (25–300°C) and W_2 (300–600°C) are found in the case of DZR70.

The DTA curves of DZRx samples with $x \leq 50$ show only one intense and broad endothermic effect in the 25–300°C range. The DZR70 DTA curve shows also this effect centred at 142°C, as well as an exothermic peak at 877°C which does not correspond to any weight change in the TG curve.

The evolutions of the DZR10, DZR30 and DZR70 specific surface area as a function of the pyrolysis temperature are compared in Fig. 6. The DZRx samples with $x \leq 50$ are almost fully dense to N_2 adsorption in the xerogel state and display a relevant increase of the specific surface area at 600°C (630 $m^2 g^{-1}$ for DZR10) with a progressive collapse of porosity with further heating.[30] It is noteworthy that DZR10 maintains a specific surface area of 198 $m^2 g^{-1}$ at 1000°C. On the contrary, the DZR70 specific surface area remains quite constant throughout the whole pyrolysis process and never exceeds 15 $m^2 g^{-1}$. The increase in specific surface area at intermediate temperatures for the DZRx ($x \leq 50$) is mainly due to the formation of mesopores, as illustrated by the typical pore size distribution shown in Fig. 7.

3.3 ^{29}Si MAS NMR spectroscopy

Solid state NMR spectroscopy is a useful tool to characterise the local environment of atoms in the solid state and has been used here to identify the various Si sites in the DZRx samples treated at high temperature. The ^{29}Si MAS NMR spectra obtained on the DZR20 sample, pyrolysed at 1000 and 1400°C, are presented in Fig. 8. At 1000°C peaks at −23, −66 and −100 ppm are found corresponding to D, T and Q units in an oxycarbide phase. The low chemical shift of the Q units is quite remarkable, since this peak is usually found around −110 ppm in silicon oxycarbide glasses.[22] At 1400°C, the spectrum shows three sharp peaks

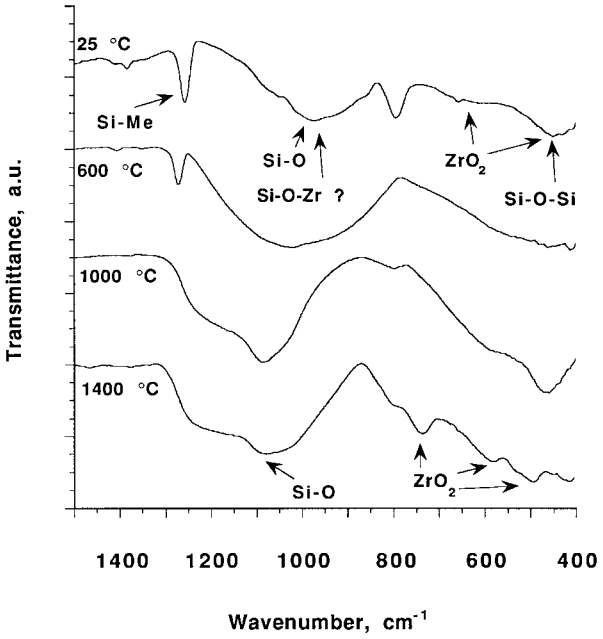

Fig. 3. Evolution with temperature of the FTIR spectra of the DZR70 samples.

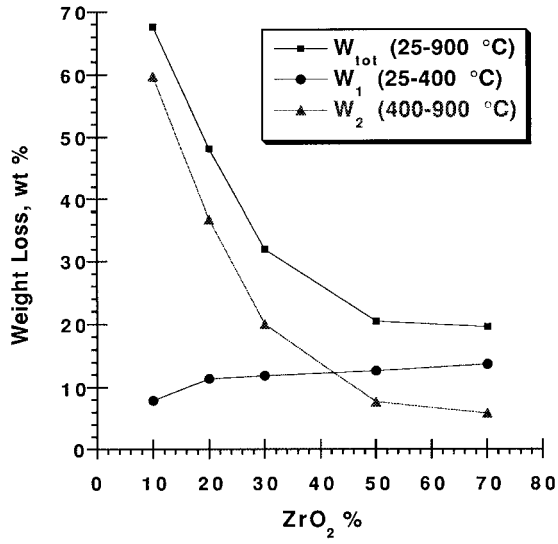

Fig. 5. Weight losses calculated from TG analyses on various DZRx samples.

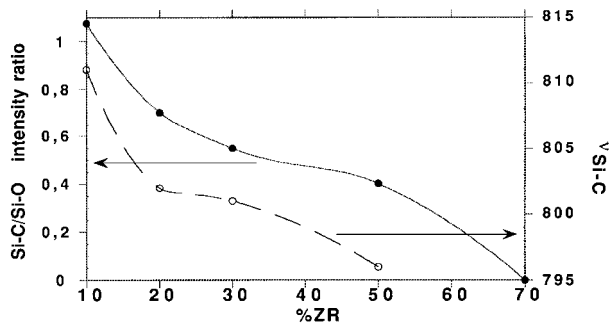

Fig. 4. Evolution versus %Zr of the relative intensities of Si–C and Si–O peaks and of the Si–C band position at 1400°C.

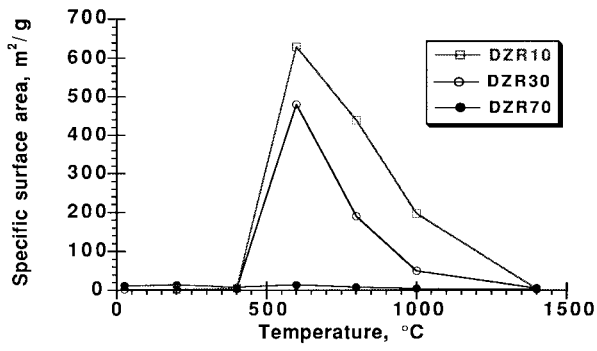

Fig. 6. Surface area evolution with pyrolysis temperature: comparison between DZR10, DZR30 and DZR70.

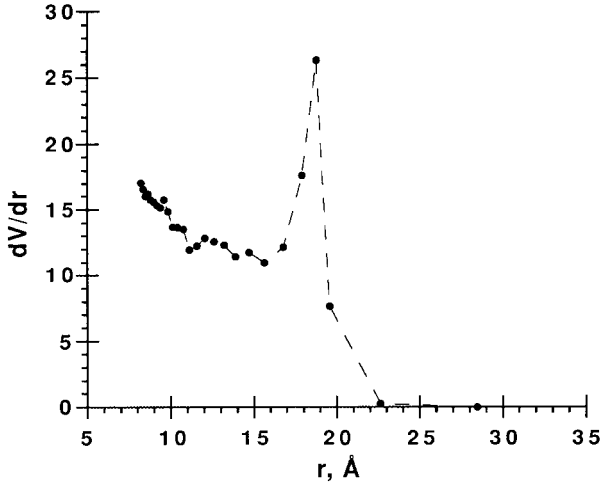

Fig. 7. Pore size distribution of DZR10 heat treated at 800°C calculated from N_2 sorption data.

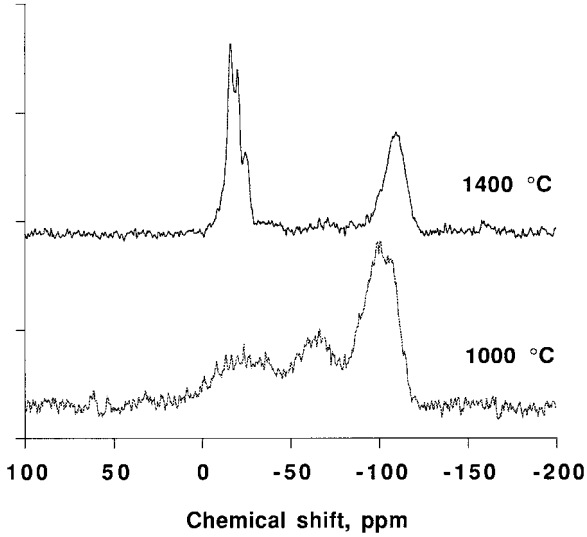

Fig. 8. ^{29}Si MAS NMR spectra of DZR20 heat treated at 1000 and 1400°C.

at −15·8, −19·7 and −24·1 ppm, attributed to the presence of well organised β and α SiC phases, as well as a broad signal at −109 ppm due to amorphous silica. For this sample, the amount of Q units, calculated by a profile fitting procedure, is 46 mol% at 1400°C. The results obtained on DZR30 at 1000°C are quite similar, whereas at 1400°C a residual oxycarbide phase is still present and the silica amount (50 mol%) increases at the expense of the SiC phases.

3.4 X-ray diffraction

All the samples treated up to 800°C display an amorphous structure, as revealed by the XRD patterns. At 1000°C, the onset of crystallisation is observed, as shown in Fig. 9. Owing to the significant peak broadening, it is very difficult to ascertain whether cubic (*c*), tetragonal (*t*) or both zirconia polymorphs are present. On the other hand, both tetragonal (*t*) and monoclinic (*m*) zirconia phases are

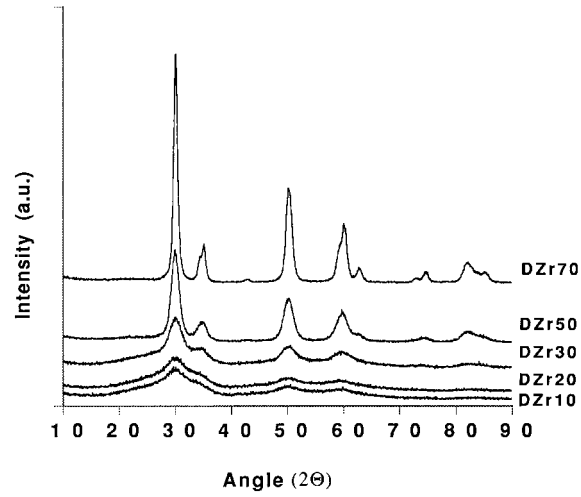

Fig. 9. XRD patterns of DZR*x* samples heat treated at 1000°C.

detected in the samples treated at 1400°C (Fig. 10). The crystallite dimensions and $m/(m+t)$ ZrO_2 ratios, calculated using a modified Rietveld method,[29] are reported in Table 2. It is noteworthy that the lowest value (≈25%) of monoclinic phase content is for the DZR30 sample. Weak haloes centred at $2\Theta \approx 20°$, assigned to the presence of amorphous SiO_2, are also visible in all samples. The presence of SiC polymorphs can not be safely ascertained owing to the superposition with more intense zirconia reflections.

3.5 Transmission electron microscopy

TEM observations were conducted on a number of powders to follow their microstructural evolution as a function of the annealing temperature.

Fully amorphous structures were found in the samples treated at temperatures ≤800°C, in agreement with the XRD results. The morphology of the DZR30 sample treated at 600°C is shown by the micrograph in Fig. 11, featuring spherical amorphous domains with an estimated diameter of 4 nm. Pores homogeneously distributed and with size ranging from 1 to 2 nm are also visible.

Figure 12 shows the bright field image of the DZR50 sample treated at 800°C and the corresponding diffraction pattern showing a typical amorphous halo. The microstructure of this sample appears to be more dense, not showing any longer the pores detected at lower temperatures. During the observations a partial crystallisation of the sample could be induced by deliberately increasing the electron beam intensity. At 1000°C, crystalline reflections were detected and crystalline particles from 2 nm up to about 30 nm were observed, as shown in Fig. 13. In agreement with the XRD data, the electron diffraction patterns confirmed the main crystalline phase to be tetragonal ZrO_2. At 1400°C, crystallisation proceeds further and

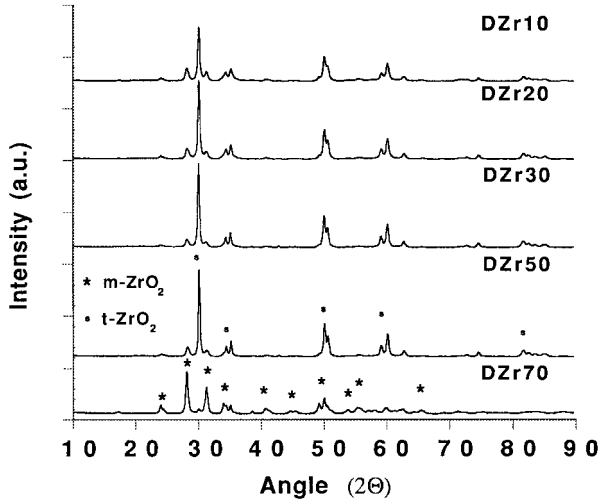

Fig. 10. XRD patterns of DZRx samples heat treated at 1400°C.

Table 2. Crystallite dimensions and m-ZrO_2 content in DZRx samples

Sample	*Crystallite dimensions (nm)*		*m/(m+t) ZrO2*
	m-ZrO₂	*t-ZrO₂*	*(vol%)*
DZR10	10·3 ± 0·4	12·6 ± 0·1	41·1
DZR20	7·3 ± 0·1	18·2 ± 0·2	34·8
DZR30	6·6 ± 0·2	17·8 ± 0·2	26·1
DZR50	7·4 ± 0·2	19·4 ± 0·2	28·9
DZR70	13·8 ± 0·2	31 ± 3	95·8

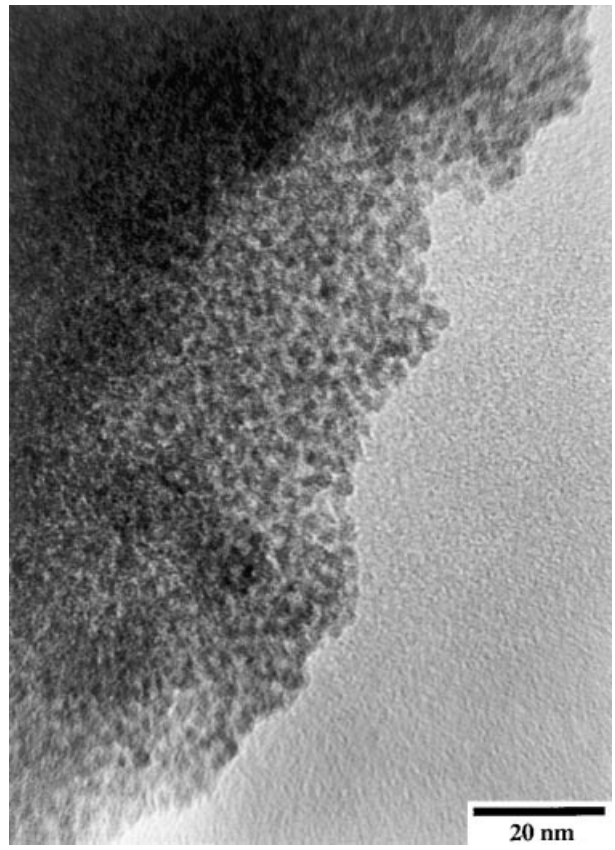

Fig. 11. Bright field image of the DZR30 sample heat treated at 600°C.

diffraction patterns due to monoclinic and tetragonal ZrO_2 phases are observed. The microstructure of the DZR50 sample treated at such temperature is shown by the TEM micrograph in Fig. 14, featuring ZrO_2 crystallites larger than those observed at 1000°C.

TEM observations, not reported herewith, were also carried out on DZR10 and DZR70 samples after heat treatments at temperatures in the 800–1400°C temperature range. Results regarding phase and crystallite size evolutions do agree in all cases with the XRD results.

4 Discussion

For ZrO_2 content up to 30 mol%, the sol–gel processing of DEDMS/$Zr(OPr^n)_4$ mixtures makes it possible to produce transparent, monolithic and compliant xerogels, which remain monolithic even after pyrolysis up to 1400°C. On the contrary, the hydrolysis-condensation process of DZR50 and DZR70 generates brittle and powdered samples. This can be related to differences in the gel structure that was found to depend strongly on the Zr content in previous studies.[15,30] For $x \leq 30$, the gel can be viewed as a nanocomposite made of long, flexible and mobile polydimethylsiloxane chains crosslinked by zirconia particles, whereas for $x > 30$, the closer proximity of the oxide particles might lead to the formation of short and constrained polysiloxane units.

The pyrolysis process can be divided into two main stages: for $T \leq 800$°C, the polymer-to-ceramics transformation occurs with loss of volatile species (Fig. 5) while for $T > 800$°C, the amorphous inorganic composites will undergo crystallisation.

4.1 The pyrolysis process up to 800°C

For DZRx ($x \leq 50$), the TG analyses show that the weight losses are completed at about 900°C, and that the total weight loss amplitude (W_{tot}) decreases versus Zr content (Fig. 5). The characterisation of DZRx pyrolysis by coupled TG–GC–MS under He atmosphere,[30] has shown that these weight losses are mainly due to evolution of siloxane oligomers: these species form out of redistribution reactions of Si–O/Si–O and Si–C/Si–O bonds occuring between siloxane units, and their structure will thus strongly depend from the nature of the Si moieties in the various composites. The presence of long polysiloxane chains in DZrx ($x \leq 30$) will give rise to higher molecular weight species (and thus higher weight losses) than in the case of DZrx ($x > 30$) for which the siloxane and zirconia species are more interconnected.

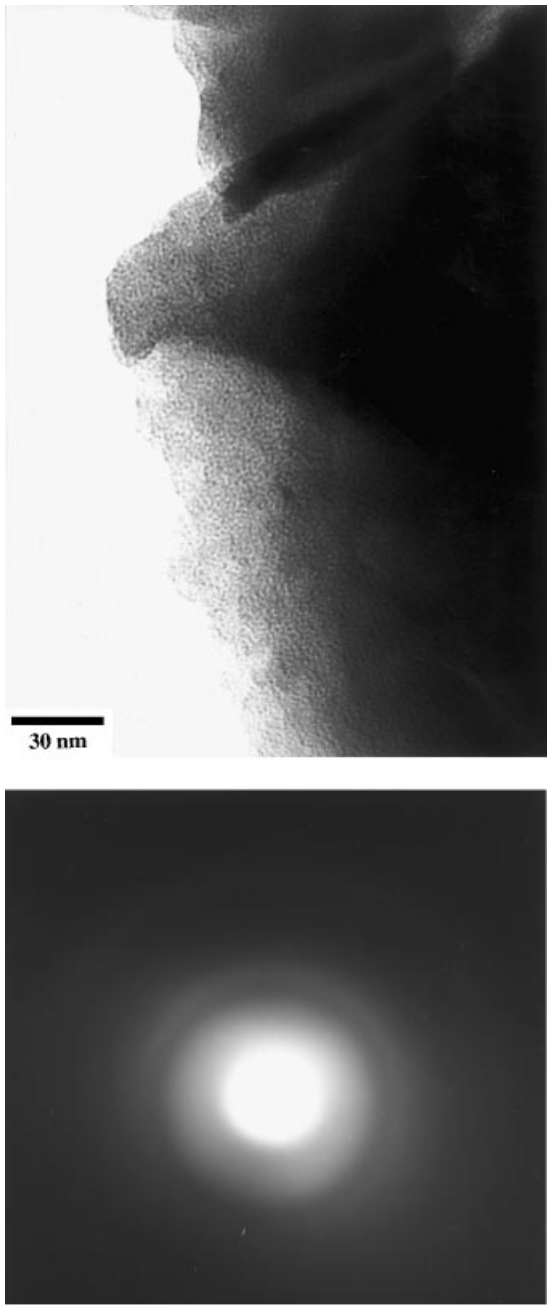

Fig. 12. Bright field image and corresponding selected area diffraction of the DZR50 sample heat treated at 800°C.

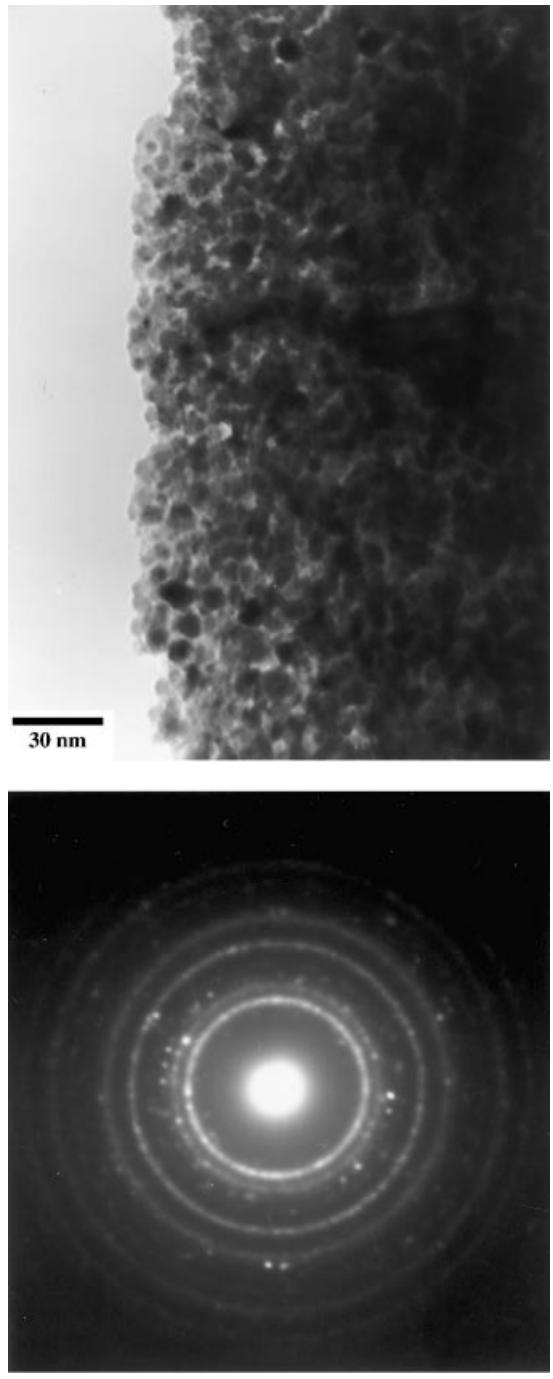

Fig. 13. Bright field image and selected area diffraction pattern of the DZR50 sample heat treated at 1000°C.

These differences in weight losses are affecting the microstructures of the various samples as shown from the porosity measurements (Fig. 6). The porosity of DZRx xerogels is very low. For $x \leq 50$, the significant evolution of gaseous species during the pyrolysis generates intermediates characterised by high specific surface area. At 600–800°C, the specific surface area decreases with Zr content, according to the weight losses trends (W_2 and W_{tot}) shown in Figure 5. The highest surface area value at 600°C is presented by DZR10 with $630\,m^2\,g^{-1}$. The production of mesoporous materials in this temperature range is confirmed by both TEM and N_2 sorption results (Figs 11 and 7). The specific surface area then reduces above 800°C and further heating at 1400°C leads to almost dense materials. A different behavior is observed for DZR70: this sample displays a low surface area throughout the whole pyrolysis process, as a consequence of a different pyrolysis pathway. Indeed, the weight change is already finished at 600°C and is characterised by the lowest weight loss above 300°C. This thermal behaviour is most likely related to the formation of a highly interconnected network between the D silicon units and the zirconia counterpart in the gel. This structural organisation accounts for the low frequency shift observed for the Si–O stretching vibrations in the DZR70 xerogel spectrum (Figure 3), which is probably determined by the contribution of Si–O–Zr

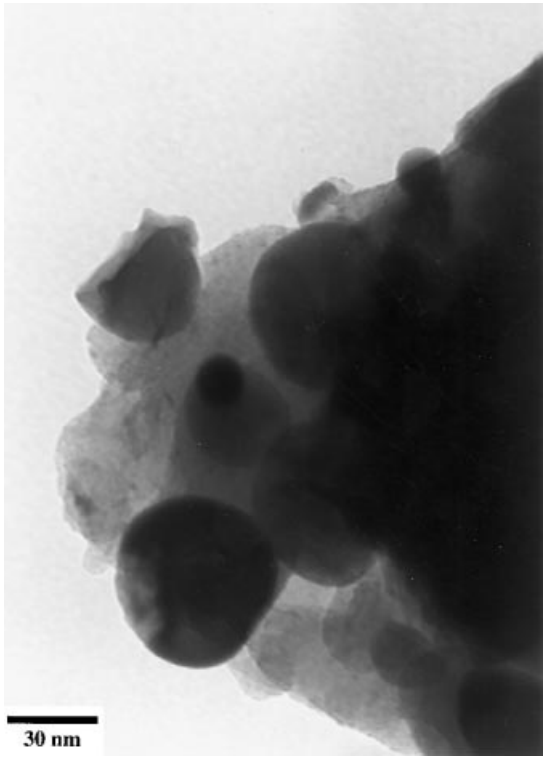

Fig. 14. Bright field image of the DZR50 sample heat treated at 1400°C.

absorptions. In such crosslinked structure, the silicon derived moiety will not easily undergo redistribution reactions, but just decompose to transform in low molecular weight volatiles or segregate as free carbon.

4.2 The phase evolution between 800 and 1400°C

The DZR*x* samples are all amorphous up to 800°C from XRD and TEM analyses. At 1000°C, crystalline features attributed to the presence of tetragonal zirconia are present in both X-ray and electron diffraction patterns, according to the general behaviour observed for sol–gel derived zirconia.[35] The crystalline reflections are comparatively weak for the DZR*x* samples with lower Zr content (Fig. 9), whereas DZR70 is characterised by more intense and sharper diffraction peaks. Accordingly, a well defined crystallisation peak at 870°C is present in the DTA curve for the DZR70. It is noteworthy that, even in the xerogel state, the infrared spectrum of DZR70 shows a more organised zirconium environment as compared to the features exhibited by other DZR*x* samples. This behavior is conserved throughout the whole thermal process. In the infrared spectrum of DZR70 heated at 1400°C (Fig. 3), the characteristic bands due to a crystalline ZrO_2 polymorph could be well detected. At 1400°C, the predominant crystalline phase in DZR70 is monoclinic ZrO_2, according to TEM and XRD results. The DZRx samples with $x \leq 50$, are characterised at 1400°C by the presence of a prevailing tetragonal phase, featuring increasing average crystallite dimensions with increasing zirconium content. The maximum estimated crystallite size for the DZR50 is 19 nm. The formation of a stable *t*-ZrO_2 phase, in the absence of stabilisation with divalent or trivalent cations, requires that the crystallite mean size stays below 30 nm, approximately.[36] Therefore, in the DZR70, the preferential martensitic transformation from tetragonal to monoclinic phase should take place because of crystallite size exceeding this value (Table 2).

The silicon-based matrix undergoes an important structural rearrangement during the pyrolysis process up to 800°C. As shown by ^{29}Si MAS NMR (Fig. 8), the thermal evolution leads at 1000°C to the formation of D, T and Q units in a silicon oxycarbide phase. The low chemical shift presented by the Q units at 1000°C is quite remarkable. According to reported results for amorphous SiO_2–ZrO_2 mixtures prepared to obtain zircon[37] and SiO_2–ZrO_2 gels prepared by a non-hydrolytic route,[38] the peak at −100 ppm, attributed to the Q units, should account for the presence of Si–O–Zr bonds.

The presence at high temperature of heterometallic bonds between zirconium and silicon atoms should lead to a strong matrix effect on the crystallisation of the zirconia polymorphs. Differences between structural arrangements between the ZrO_2 particles and the siloxane moiety in DZR*x* gels have already been pointed out and related to different pyrolysis pathways below 800°C.[30] A highly interconnected network between D units and ZrO_2 based particles has been proposed in the case of DZR70. Consequently, these differences in DZRx matrices should have different influences on the *t*-$ZrO_2 \rightarrow$ *m*-ZrO_2 martensitic transformation[39] resulting in the observed different crystallisation pathways.

The gel chemical composition plays a major role also in determining the pyrolysis products of the silicon counterpart. The infrared spectra at 1400°C point out that a decreasing amount of silicon carbide phase is obtained with increasing Zr content. This result is in good agreement with the quantitative analysis of silicon units obtained from NMR spectra at 1400°C. In comparison with the DZR20 sample which is characterised by well organised β and α SiC and amorphous silica, the DZR30 displays a residual amorphous oxycarbide phase and an increased amount of silica. These results suggest a more difficult separation of pure silicon carbide with increasing Zr content. The NMR spectra show well organised SiC phases. Unfortunately, XRD and TEM results can not provide direct indications for the presence of SiC polymorphs, as silicon carbide and zirconia reflections strongly overlap. However, preliminary quantitative phase

calculations from XRD spectra (R. Ceccato and L. Lutterotti, unpublished results) are in good agreement with the quantitative evaluation obtained from NMR in the case of DZR20 and DZR30 and indicate the decrease of the SiC amount with increasing Zr content. The inhibition of SiC crystallisation can be ascribed to the preferential loss of carbon due to the Si–C bond breaking observed during the pyrolysis of DZRx samples with higher Zr content. As a matter of fact, methane evolution was observed to increase with increasing Zr content,[30] and it was the predominant species to evolve during the DZR50 pyrolysis process.[30] Moreover, taking into account the presence of a residual amorphous oxycarbide phase in the DZR30 at 1400°C, the occurrence of an increasing amorphous SiC_xO_{4-x} structure with increasing ZrO_2 content can be inferred.

5 Conclusions

Polydimethylsiloxane–zirconia nanocomposites with different ZrO_2 contents were prepared by a sol–gel route. Thermoanalytical investigations were conducted to identify the temperature ranges for the main transformations and reactions. The microstructural changes induced by thermal treatments, carried out from 400 to 1400°C, were followed with several experimental techniques.

At 600–800°C, the pyrolysis process generates highly porous amorphous materials characterised by the formation of mesopores and specific surface area as high as $630\,m^2\,g^{-1}$, in the case of DZR10. The remarkable porosity observed at high temperature, particularly in the case of DZR10, makes these matrices suitable for such applications as adsorbents, sensors and catalyst supports.

The ceramisation process of the polydimethylsiloxane–zirconia gels leads at 1000°C to the formation of Si–C–O/ZrO_2 nanocomposites composed of amorphous silicon oxycarbide matrix featuring finely dispersed *t*-ZrO_2 crystallites.

At higher temperature, i.e. 1400°C, the monoclinic polymorph is also observed, though its amount stays well below the amount of tetragonal phase for ZrO_2 content $\leq$50 mol%. Indications for the presence of α and β SiC phases after treatments at 1400°C come from solid state NMR analyses. The formation of the silicon carbide phase appears more difficult for increasing Zr contents in the gel.

Acknowledgements

MURST 40% is kindly acknowledged for the financial support.

References

1. Brinker C. J. and Scherer, G. W., *Sol–Gel Science*, Academic Press, San Diego, CA, 1990, chapter 12.
2. Carturan, G., Facchin, G., Gottardi, V. and Navazio, G., Preparation of supports for catalysis by the gel route. *J. Non-Cryst. Solids*, 1984, **63**, 273–278.
3. Blanchard, N., Boilot, J. P., Colomban, Ph. and Pouxviel, J. C., New glasses from metal-organic precursors: preparation and properties. *J. Non-Cryst. Solids*, 1986, **82**, 205–209.
4. Babonneau, F., Dirè, S., Bonhomme-Coury, L. and Livage, J., Sol–gel synthesis of heterometallic oxopolymers. In *Inorganic and Organometallic Polymers II*, ed. P. Wisian-Neilson, H. R. Allcock and K. J. Winne. ACS, Washington, DC, 1994, chapter 12, pp. 134–148.
5. Schmidt, H., Aspects of chemistry and chemical processing of organically modified ceramics. *Mat. Res. Soc. Symp. Proc.*, 1990, **180**, 961–973.
6. Schmidt, H., Inorganic-organic composites by sol–gel techniques. *J. Sol–Gel Sci. Technol.* **1** (1994) 217–31 and references therein.
7. Wang, B. and Wilkes, G. L., New Ti-PTMO and Zr-PTMO ceramer hybrid materials prepared by the sol–gel method: synthesis and characterization. *J. Polymer Sci. A*, 1991, **29**, 905–909.
8. Wen, J. and Wilkes, G. L., Organic-inorganic hybrid network materials by the sol–gel approach. *Chem. Mater.* **8** (1996) 1667–1681 and references therein.
9. Sorarù, G. D., D'Andrea, G., Campostrini, R. and Babonneau, F., Characterization of methyl-substituted silica gels with Si–H functionalities. *J. Mater. Chem.*, 1995, **5**, 1363–1374.
10. Dirè, S., Pagani, E., Babonneau, F., Ceccato, R. and Carturan, G., Unsupported SiO_2-based organic–inorganic membranes. Part 1: synthesis and structural characterization. *J. Mater. Chem.*, 1997, **7**, 67–73.
11. Diré, S., Bois, L., Babonneau, F. and Carturan, G., Spectroscopic characterization of mixed siloxane–oxide systems. *Polymer Prepr.*, 1991, **32**, 501–502.
12. Diré, S., Babonneau, F., Sanchez, C. and Livage, J., Sol–gel synthesis of siloxane–oxide hybrid coatings ($Si(CH_3)_2O$–MO_x: M = Si, Ti, Zr, Al) with luminescent properties. *J. Mater. Chem.*, 1992, **2**, 239–244.
13. Diré, S., Babonneau, F., Carturan, G. and Livage, J., Synthesis and characterization of mixed siloxane-titania materials. *J. Non Cryst. Solids*, 1992, **147&148**, 62–66.
14. Babonneau, F., Bois, L., Livage, J. and Dirè, S., Structural investigation of sol–gel derived hybrid siloxane–oxide materials using ^{29}Si MAS–NMR spectroscopy. *Mat. Res. Soc. Symp. Proc.*, 1993, **286**, 289–294.
15. Babonneau, F., Maquet, J. and Dirè, S., Structural characterization of sol–gel derived siloxane-zirconia materials. *Polymer Prepr.*, 1993, **34**, 242–243.
16. Babonneau, F., ^{29}Si, ^{17}O liquid NMR and ^{29}Si CP–MAS NMR characterization of siloxane-oxide materials, [$(CH_3)_2SiO/TiO_2$, $(CH_3)_2SiO/ZrO_2$]. *Mat. Res. Soc. Symp. Proc.*, 1994, **346**, 949–960.
17. Schaudel, B., Guermeur, C., Sanchez, C., Nakatani, K. and Delaire, J. A., Spirooxazine- and spiropyran-doped hybrid organic–inorganic matrices with very fast photochromic responses. *J. Mater. Chem.*, 1997, **7**, 61–65.
18. Schmidt, H. and Seiferling, B., Chemistry and applications of inorganic-organic polymers. *Mat. Res. Soc. Symp. Proc.*, 1986, **73**, 739–750.
19. Schmidt, H. and Wolter, H., Organically modified ceramics and their applications. *J. Non Cryst. Solids*, 1990, **121**, 428–435.
20. Dirè, S., Pagani, E., Ceccato, R. and Carturan, G., Unsupported SiO_2-based organic-inorganic membranes. Part 2: surface features and gas permeation. *J. Mater. Chem.*, 1997, **7**, 919–922.
21. Zhang, H. and Pantano, C. G., Synthesis and characterization of silicon oxycarbide glasses. *J. Am. Ceram. Soc.*, 1990, **73**, 958–963.

22. Babonneau, F., Sorarù, G. D., D'Andrea, G., Dirè, S. and Bois, L., Silicon oxycarbide glasses from sol–gel precursors. *Mat. Res. Soc. Symp. Proc.*, 1992, **271**, 789–794.
23. Sorarú, G. D., Sglavo, V. M., Dirè, S., D'Andrea G. and Babonneau, F., High strenght, high modulus silicon-oxycarbide glasses. In *3rd Euroceramics*, vol. 2, ed. P. Duran, J. P. Fernandez. Faenza Ed. Iberica, 1993. pp. 1157–1162.
24. Babonneau, F., Bois, L. and Livage, J., Silicon oxycarbides via sol–gel route: characterization of the pyrolysis process. *J. Non-Cryst. Solids*, 1992, **147&148**, 280–284.
25. Bois, L., Maquet, J., Babonneau, F., Mutin, H. and Bahloul, D., Structural characterization of sol–gel derived oxycarbide glasses. 1. Study of the pyrolysis process. *Chem. Mater.*, 1994, **6**, 796–802.
26. Chen, K. C., Thorne, K., Chemseddine, A., Babonneau, F. and Mackenzie, J. D., Silicon carbide via the hydrolysis–condensation process of dimethyldiethoxysilane/tetraethoxysilane copolymers. *Mat. Res. Soc. Symp. Proc.*, 1988, **121**, 571–574.
27. Burns, G. T., Taylor, R. B., Xu, Y., Zangvil, A. and Zank, G. A., High temperature chemistry of the conversion of siloxanes to silicon carbide. *Chem. Mater.*, 1992, **4**, 1313–1323.
28. Dirè, S. and Babonneau, F., Structural evolution during pyrolysis of sol–gel derived hybrid materials. *J. Sol–Gel Sci. Technol.*, 1994, **2**, 139–142.
29. Lutterotti, L., Scardi, P. and Maistrelli, P., LS1—a computer program for simultaneous refinement of material structure and microstructure. *J. Appl. Cryst.*, 1992, **25**, 459–462.
30. Dirè, S., Campostrini, R. and Ceccato, R., Pyrolysis chemistry of sol–gel derived polydimethylsiloxane–zirconia nanocomposites. The influence of zirconium on polymer-to-ceramic conversion. *Chemistry of Materials*, 1998, **10**(1), 268–278.
31. Nogami, M., Glass preparation of the ZrO_2–SiO_2 system by the sol–gel process from metal alkoxides. *J. Non-Cryst. Solids*, 1985, **69**, 415–423.
32. Abe, Y., Sugimoto, N., Nagao, Y. and Misono, T., Preparation of monolithic gels SiO_2–M_xO_y (M = Al, Zr) by the reaction of silicic acid with metal chelate compounds. *J. Non-Cryst. Solids*, 1989, **108**, 150–156.
33. Launer, P. J., Infrared analysis of organosilicon compounds: spectra–structure correlations. In *Silicon Compounds*, Petrarch Systems Inc., Karlsruhe, 1984, pp. 69–72.
34. Miranda Salvado, I. M., Serna, C. J. and Fernandez Navarro, J. M., ZrO_2–SiO_2 materials prepared by sol–gel. *J. Non-Cryst. Solids*, 1988, **100**, 330–338.
35. Srinivasan, R., De Angelis, R. J., Ice, G. and Davis, B. H., Identification of tetragonal and cubic structures of zirconia using synchroton X-radiation source. *J. Mater. Res.*, 1991, **6**, 1287–1292.
36. Garvie, R. C., The occurrence of metastable tetragonal zirconia as a crystallite size effect. *J. Phys. Chem.*, 1965, **69**, 1238–1243.
37. Hartman, J. S., Millard, R. L. and Vance, E. R., A ^{29}Si magic angle spinning NMR and DTA study of thermal crystallization of sphene and zircon gels. *J. Mater. Sci.*, 1990, **25**, 2785–2890.
38. Andrianainarivelo, M., Corriu, R., Leclercq, D., Mutin, P. H. and Vioux, A., Mixed oxides SiO_2–ZrO_2 and SiO_2–TiO_2 by a non-hydrolytic sol–gel route. *J. Mater. Chem.*, 1996, **6**, 1665–1671.
39. Nogami, M. and Tomozawa, M., ZrO_2-transformation-toughened glass-ceramics prepared by the sol–gel process from metal alkoxides. *J. Am. Ceram. Soc.*, 1986, **69**, 99–102.